

Thermal fading of the $1/k^4$ -tail of the momentum distribution induced by the hole anomaly

Giulia De Rosi,^{1,*} Grigori E. Astrakharchik,^{1,2,†} Maxim Olshanii,³ and Jordi Boronat^{1,‡}

¹*Departament de Física, Universitat Politècnica de Catalunya, Campus Nord B4-B5, 08034 Barcelona, Spain*

²*Departament de Física Quàntica i Astrofísica, Facultat de Física, Universitat de Barcelona, E-08028 Barcelona, Spain*

³*Department of Physics, University of Massachusetts Boston, Boston Massachusetts 02125, USA*

(Dated: February 21, 2024)

We study the thermal behavior of correlations in a one-dimensional Bose gas with tunable interaction strength, crossing from weakly-repulsive to Tonks-Girardeau regime. A reference temperature in this system is that of the hole anomaly, observed as a peak in the specific heat and a maximum in the chemical potential. We find that at large momenta k and temperature above the anomaly threshold, the tail C/k^4 of the momentum distribution (proportional to the Tan contact C) is screened by the $1/|k|^3$ -term due to a dramatic thermal increase of the internal energy emerging from the thermal occupation of spectral excitation states. The same fading is consistently revealed in the behavior at short distances x of the one-body density matrix (OBDM) where the $|x|^3$ -dependence disappears for temperatures above the anomaly. We obtain a new general analytic tail for the momentum distribution and a minimum k fixing its validity range, both calculated with exact Bethe-Ansatz method and valid in all interaction and thermal regimes, crossing from the quantum to the classical gas limit. Our predictions are confirmed by comparison with ab-initio Path Integral Monte Carlo calculations for the momentum distribution and the OBDM exploring a wide range of interaction strength and temperature. Our results unveil a novel connection between excitations and correlations. We expect them to be of interest to any cold atomic, nuclear, solid-state, electronic and spin system exhibiting an anomaly or a thermal second-order phase transition.

Tan relation $n(k) \sim C/k^4$ describes the tail of the momentum distribution $n(k)$ at high momenta k and its amplitude is fixed by the Tan contact parameter C [1–3]. This universal law is valid for a broad range of quantum systems, from nucleons [4] to ultracold atoms [5, 6], of bosonic and fermionic statistics, with any interaction strength and particle number [3]. It applies to multicomponent systems [7, 8] and in arbitrary conditions of confinement [5, 9, 10] and spatial dimensionality [6, 11, 12]. It provides a key connection between microscopic large-momenta (short-distance) correlations and macroscopic thermodynamic quantities such as C [13].

Tan relation is based on the assumption that the tail of the momentum distribution depends entirely on contact two-body interactions [1–3, 13] which are modelled only by the universal s -wave scattering length [14] entering into C . $n(k) \sim C/k^4$ holds then whenever the interaction range r_0 is negligible compared to all other relevant length scales of the problem, including the average interparticle distance d and the thermal de Broglie wavelength $\lambda = \sqrt{2\pi\hbar^2/(mk_B T)}$. Tan law is valid for momenta much larger than the average momentum of particles $d^{-1}, \lambda^{-1} \ll |k| \ll r_0^{-1}$. The present work provides a precise estimate for the minimum momentum k_{\min} above which the tail of the distribution is defined $k_{\min} \lesssim |k|$. This new k_{\min} holds for any interaction strength and temperature.

Tan relation was believed to be well justified in ultracold atomic gases due to their extreme diluteness and low temperatures. Recently, possible violations to the Tan relation have been found in the presence of spin-orbit coupling [15], particle losses [16], impurity-bath interactions in an expanding gas [17] and hard-wall boundaries [18]. Tan law has been considered valid at temperatures T even well above the critical value T_c of the superfluid phase transition [13, 14, 19], in contrast with the Maxwell-Boltzmann Gaussian decay expected in the classical gas limit. Tan relation has been experimentally confirmed only at $T < T_c$ [20], raising the question above which

temperature it may be *violated* [21].

Atomic, solid-state, electronic and spin systems exhibit an *Anomaly*, i.e., a thermal feature in the thermodynamic properties as a function of temperature, identified by a peak in the specific heat, a maximum in the chemical potential or a minimum in the magnetization, located at the anomaly temperature T_A [22]. The onset of a thermal second-order phase transition is signalled by an anomaly where $T_A = T_c$ [23]. In absence of a phase transition, the anomaly is due to unpopulated states in the excitation spectrum [24–30]. When the temperature is comparable to T_A , empty spectral states are thermally occupied, the excitations experience the breakdown of the low- T quasiparticle description [31], and thermal fluctuations dominate over quantum correlations at $T > T_A$ [22]. Thus, the internal energy is almost constant with temperature at $T < T_A$, and rapidly increases at $T > T_A$ [32]. Anomalies are present [22] in any system in one spatial dimension (1D) [33–37] where phase transitions are forbidden [23].

In a 1D repulsive Bose gas, the *Hole Anomaly* has been recently predicted for any contact interaction strength [22]. This mechanism occurs through the thermal occupation of states located below the spectral hole branch whose maximum provides the energy scale for the anomaly temperature T_A . Tan relation is confirmed by comparison with Path Integral Monte Carlo (PIMC) results at $T < T_A$ [38]. No knowledge at $T > T_A$ was available so far and an open question is how the tail of the momentum distribution $n(k)$ changes across T_A .

In this work, we report that the thermal increase of the internal energy, induced by the hole anomaly, makes dominant the $1/|k|^3$ -term, by screening the Tan relation $n(k) \sim C/k^4$ at $T > T_A$. This thermal fading occurs for any interaction strength at high temperatures as shown by PIMC results. It may be observed in 1D atomic Bose gases where $n(k)$ has been measured [39–42] and the exploration of a wide range of interaction strength and temperature values is possible [43].

Model.— We consider a 1D uniform gas composed of N Bose particles interacting via contact-pairwise repulsive potential and described by the Hamiltonian [44]:

$$H = -\frac{\hbar^2}{2m} \sum_{i=1}^N \frac{\partial^2}{\partial x_i^2} + g \sum_{i>j}^N \delta(x_i - x_j), \quad (1)$$

where m is the particle mass, $g = -2\hbar^2/(ma) > 0$ is the 1D coupling constant [45], and $a < 0$ is the 1D s -wave scattering length. We study the thermodynamic limit $N \rightarrow \infty$ by increasing the system size $L \rightarrow \infty$ while keeping the linear density $n = N/L$ fixed. The interaction strength is $\gamma = -2/(na)$.

In 1D, there are no phase transitions but rather a continuous crossover that encompasses different regimes in terms of γ and temperature. The gas admits a mean-field description [14] in the Gross-Pitaevskii limit of weak repulsion $\gamma \ll 1$, which in 1D corresponds to high density $n|a| \gg 1$. In the Tonks-Girardeau regime of infinite repulsion $\gamma \rightarrow \infty$, achieved at low density $n|a| \rightarrow 0$, bosons become impenetrable and the wavefunction is mapped [46] onto that of an ideal (non-interacting) Fermi gas, resulting in identical thermodynamics and spectrum. Many experiments explored this interaction crossover in ultracold atom platforms [47–53]. At zero temperature, the energetic properties can be obtained using the exact Bethe-Ansatz method [14, 54–56]: the ground-state energy E_0 , chemical potential $\mu_0 = (\partial E_0/\partial N)_{a,L}$ and speed of sound $v = \sqrt{n/m(\partial\mu_0/\partial n)_a}$ which are all functions of γ .

At finite temperature T , the exact thermal Bethe Ansatz (TBA) approach [57, 58] can be used and the thermodynamics within the canonical ensemble is captured by the Helmholtz free energy $A = E - TS$, where E is the internal energy and S the entropy. The Tan contact can be obtained via [59–61]

$$\mathcal{C} = (4m/\hbar^2) (\partial A/\partial a)_{T,N,L}, \quad (2)$$

which provides information on the interaction energy and a relation between the pressure and E [1–3, 5, 6, 61, 62].

In Fig. 1, we report the exact thermal Bethe-Ansatz results of the internal energy per particle E/N as a function of temperature and for characteristic values of the interaction strength γ . We show energies in units of the Fermi value $E_F = k_B T_F = \hbar^2 \pi^2 n^2 / (2m)$ and temperatures rescaled by the quantum degeneracy threshold $T_d = T_F/\pi^2$. Vertical lines denote the hole-anomaly temperature T_A/T_d estimated from the peak in the specific heat [22]. For any γ , E/N is almost constant at $T \lesssim T_A$, while it exhibits an intense monotonic increase at $T > T_A$, due to the thermal occupation of spectral states which is completed around T_A [22].

One-Body Density Matrix.— The one-body density matrix (OBDM) is defined as the non-diagonal density [14]:

$$g_1(x = x_1 - x_2) = \langle \hat{\psi}^\dagger(x_1) \hat{\psi}(x_2) \rangle, \quad (3)$$

where $\hat{\psi}(x)$ is the Bose field, x the interparticle distance, and $\langle \dots \rangle$ the average over an ensemble in thermal equilibrium. The OBDM quantifies the coherence and corresponds

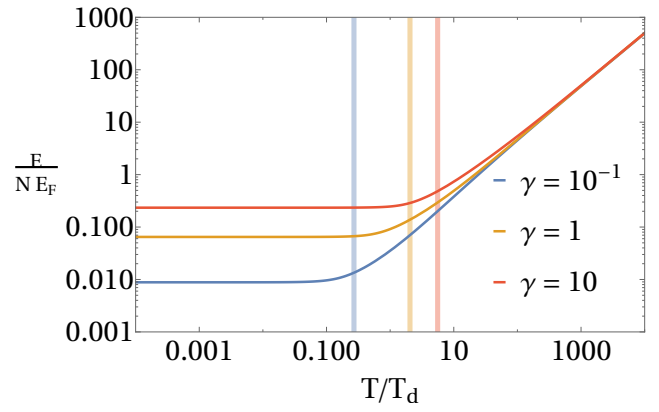


Figure 1. Internal energy per particle E/N , normalized to the Fermi value $E_F = k_B T_F = \hbar^2 \pi^2 n^2 / (2m)$, vs temperature in units of the quantum degeneracy threshold $T_d = T_F/\pi^2$ and for several interaction strengths γ reported from small (bottom) to large (top) values. Calculations have been performed with TBA. Vertical lines denote the anomaly temperature T_A/T_d from small (left) to large (right) γ , corresponding to 0.27 ($\gamma = 10^{-1}$), 2.05 ($\gamma = 1$) and 5.58 ($\gamma = 10$).

to the amplitude of the process where a particle is annihilated at position x_2 and another one is created at x_1 . At $x = 0$, one recovers the diagonal density n . The momentum distribution is the Fourier transform of the OBDM.

We employ the PIMC method to calculate the complete x -dependence of the OBDM for a wide range of interaction strength γ and temperatures in a 1D Bose gas [62]. At high temperatures, $T \gg T_d$, PIMC results show an excellent agreement with the Maxwell-Boltzmann (MB) Gaussian law $g_1(x)_{\text{MB}} = n e^{-x^2/(2\sigma^2)}$ [62] describing a classical gas and decaying to zero for $x \gg \sigma$ where $\sigma = \lambda/\sqrt{2\pi}$ is the standard deviation proportional to the thermal de Broglie wavelength λ .

The short-distance expansion of the OBDM is [63]

$$\frac{g_1(|x| \lesssim x_{\text{max}})}{n} = 1 + \sum_{i=1}^{\infty} c_i (xn)^i + b_3 |xn|^3 + \mathcal{O}(|xn|^4). \quad (4)$$

The coefficients c_i in the Taylor expansion of the analytic part are the corresponding moments of the momentum distribution [63], they diverge for $i > 3$ and the odd ones vanish $c_1 = c_3 = \dots = 0$. From the Hellmann-Feynman theorem [64], one finds that the second coefficient is a function of the internal energy E/N and Tan contact \mathcal{C}/N per particle:

$$c_2 = -\frac{1}{2} \left(\frac{E}{N} \frac{2m}{\hbar^2 n^2} - \frac{\mathcal{C}}{N} \frac{1}{\gamma n^3} \right), \quad (5)$$

and c_2 can be also expressed in terms of the average kinetic energy [14, 62]. The non-analytic part of Eq. (4) starts with a $|x|^3$ dependence whose coefficient depends on \mathcal{C}/N only:

$$b_3 = (\mathcal{C}/N) / (12n^3). \quad (6)$$

At $T = 0$, Eqs. (4-6) have been derived [5] also including the coefficient of the $|x|^4$ term [65–67]. The finite-temperature

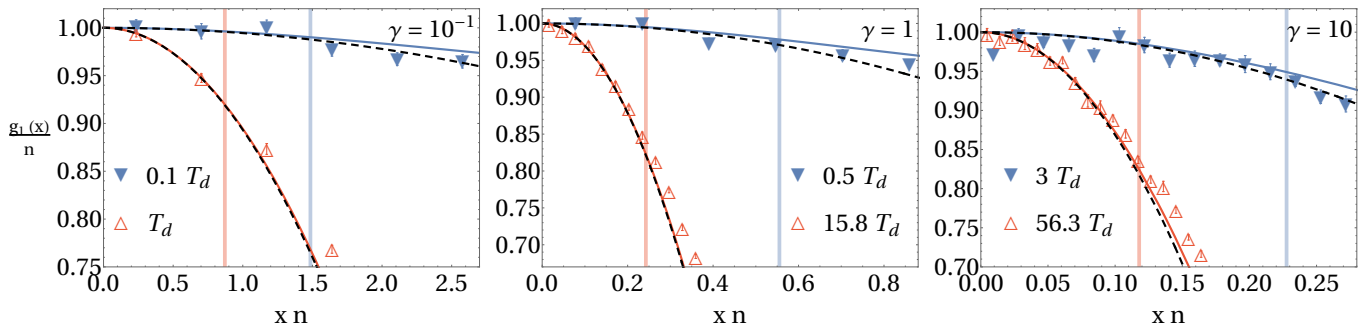


Figure 2. OBDM $g_1(x)/n$ vs interparticle distance xn (n is the density) for the interaction strength $\gamma = 10^{-1}$ (first panel), $\gamma = 1$ (second), and $\gamma = 10$ (last). Symbols denote PIMC results and their sizes are larger than the statistical error bars. Solid (empty) symbols correspond to temperatures below (above) the anomaly value T_A , Fig. 1. Solid lines represent the short-distance expansion (4) calculated with TBA. Dashed black lines correspond to Eq. (4) with $b_3 = 0$. Curves are reported from low (top) to high (bottom) temperatures in each panel. The maximal distance of the expansion $x_{\max}n$ (7) is shown with vertical lines from low (right) to high (left) temperatures at fixed γ .

dependence enters in E and C which can be evaluated with exact TBA [57, 58, 61, 62]. Eq. (4) is valid for any value of γ and T as shown by comparison with PIMC calculations [62].

We find in this work that (4) holds up to a maximal distance

$$x_{\max} = (\xi^{-1} + \sigma^{-1})^{-1} \quad (7)$$

which is determined by the healing length $\xi = \hbar/(\sqrt{2}mv)$ and the standard deviation σ of the Gaussian $g_1(x)_{\text{MB}}$. At $T = 0$, the expression (7) reduces to $x_{\max} = \xi$ which constrains the high-momentum range for the tail of the momentum distribution $n(|k| \gtrsim \xi^{-1})$ for any interaction strength, as shown previously by comparison with exact Monte Carlo results [68]. Equation (7) holds in any system where the sound velocity v , entering in ξ and depending on the interaction strength [14], is well-defined. At very high temperatures, where the system approaches the Maxwell-Boltzmann regime, we recover the classical ideal gas limit $x_{\max} = \sigma$. Equation (7) is a smooth interpolation between zero- and high-temperature limits, given by ξ and σ , respectively. Equation (7) provides an excellent approximation, for any interaction strength and temperature, of the threshold where the short-distance expansion (4) deviates from the exact PIMC results for the OBDM, as discussed below.

In Fig. 2, we show exact Path Integral Monte Carlo results of the one-body density matrix. Solid symbols correspond to temperatures below the hole anomaly $T < T_A$, while empty ones for $T > T_A$, see Fig. 1. Weakly- ($\gamma = 10^{-1}$, first panel), intermediate- ($\gamma = 1$, second) and strongly- ($\gamma = 10$, last) interacting regimes are reported. We test the importance of the non-analytic contribution by comparing the short-distance OBDM, Eq. (4), with $b_3 \neq 0$ (colored solid lines) and $b_3 = 0$ (black dashed), calculated with thermal Bethe-Ansatz. The maximal distance x_{\max} (7) is shown with vertical lines.

Our results are valid for any interaction strength γ . The short-range expansion (4) of the OBDM holds at distances limited by the upper bound (7) ($|x| \lesssim x_{\max}$) at any temperature [69], as witnessed by the comparison with PIMC findings. The non-analytic term (with coefficient b_3) plays a role

in (4) at distances close to x_{\max} for an accurate description at $T < T_A$, while it is negligible at $T > T_A$ [69]. The reason is that the internal energy increases at $T > T_A$, see Fig. 1, making b_3 (6) small compared to c_2 (5). The thermal fading of the $|x|^3$ -dependence in the short-distance OBDM is then driven by the hole anomaly. It is a crossover [69] and not an abrupt change which is expected crossing the critical temperature of a second-order phase transition.

In the high-temperature MB regime [69], we obtain $x_{\max} = \sigma$; $E/N = k_B T/2$ as the energy is defined by thermal fluctuations [22] and contact $C = 0$ as interactions are negligible, Eq. (2). The short-range behavior (4) of the OBDM recovers the analytic terms of the expansion of the Gaussian $g_1(x \lesssim \sigma)_{\text{MB}}/n = 1 - (x/\sigma)^2/2 + \mathcal{O}(x^4)$, where the non-analytic one is absent. Even though b_3 (6) can be omitted at $T > T_A$, C also enters into c_2 (5) and still plays a role until very high temperatures are reached, where $g_1(x)_{\text{MB}}$ is valid.

Momentum Distribution.— The momentum distribution is related to the OBDM (3) by a Fourier transform [14]

$$n(k) = \frac{1}{n} \int_{-\infty}^{+\infty} \frac{dx}{2\pi\hbar} \cos(k \cdot x) g_1(x), \quad (8)$$

and gives the probability to find an atom with momentum k .

In a 1D Bose gas, $n(k)$ has been calculated at $T = 0$ with the diffusion Monte Carlo technique [70, 71]. At finite temperature, various numerical and analytical methods have been applied but restricted to strong [38, 72] and weak [73] interactions, and temperatures below the hole anomaly [73, 74].

Our work fills an important gap: we compute $n(k)$ in a 1D Bose gas with the most advanced PIMC method, exploring all regimes from weak to strong interactions and from low to high temperatures [69]. To this aim, we apply the Fourier transform (8) to the PIMC results for the OBDM [62]. At high T , our PIMC data are captured by the Gaussian $n(k)_{\text{MB}} = \sigma/(\hbar\sqrt{2\pi}) e^{-\sigma^2 k^2/2}$ typical of a MB classical gas [69].

We derive the large- k tail of $n(k)$ by using the short-distance OBDM (4) in Eq. (8), where we integrate up to

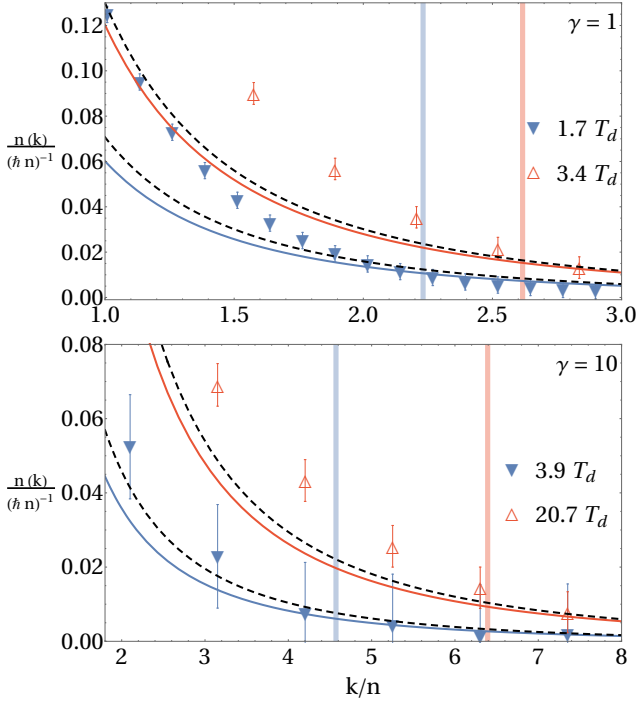


Figure 3. Momentum distribution $n(k)$ vs momentum k for $\gamma = 1$ (upper panel) and $\gamma = 10$ (lower panel). Symbols correspond to PIMC results for $T < T_A$ (solid) and $T > T_A$ (empty). Solid lines represent the tail (9) calculated with TBA. Dashed lines present (9) with $b_3 = 0$. Curves are reported from low (bottom) to high (top) temperatures in each panel. $k_{\min} = x_{\max}^{-1}$ (7) is denoted by vertical lines from low (left) to high (right) temperatures at fixed γ .

$x_{\max} = k_{\min}^{-1}$ (7) fixing the minimum momentum for the tail:

$$n(|k| \gtrsim k_{\min}) = \frac{6n^3 b_3}{\pi \hbar k^4} \left[1 - \cos\left(\frac{k}{k_{\min}}\right) \right] - \frac{1}{\pi \hbar |k|^3} \sin\left(\frac{|k|}{k_{\min}}\right) \left(2c_2 n^2 + \frac{6n^3 b_3}{k_{\min}} \right) + \mathcal{O}\left(\frac{1}{k^2}\right). \quad (9)$$

The $1/k^4$ -term emerges from the leading non-analytic behavior of the short-distance OBDM and provides the Tan relation $\sim C/k^4$, which, consistently with coordinate space, is more important at momenta closer to the lower bound $|k| \gtrsim k_{\min}$. Tan relation has been derived for the 1D Bose gas at $T = 0$ [5]. The $1/|k|^3$ -contribution depends even on the c_2 coefficient, which is a function of the internal energy and contact (5), as well as the momentum k_{\min} . Equation (9) recovers the classical limit of the Fourier transform of $g_1(x \lesssim \sigma)_{\text{MB}}$.

In Figs. 3-4, we show the correlations at large momenta and crossing the hole-anomaly temperature T_A for several interaction strengths γ . Symbols denote Path Integral Monte Carlo results for $T < T_A$ (solid) and $T > T_A$ (empty), see Fig. 1. The minimal momentum $k_{\min} = x_{\max}^{-1}$ (7) for the tail (9) is reported with vertical lines. In Fig. 3, solid and black dashed lines correspond to the tail (9) with and without the non-analytic term, respectively, and are calculated with Ther-

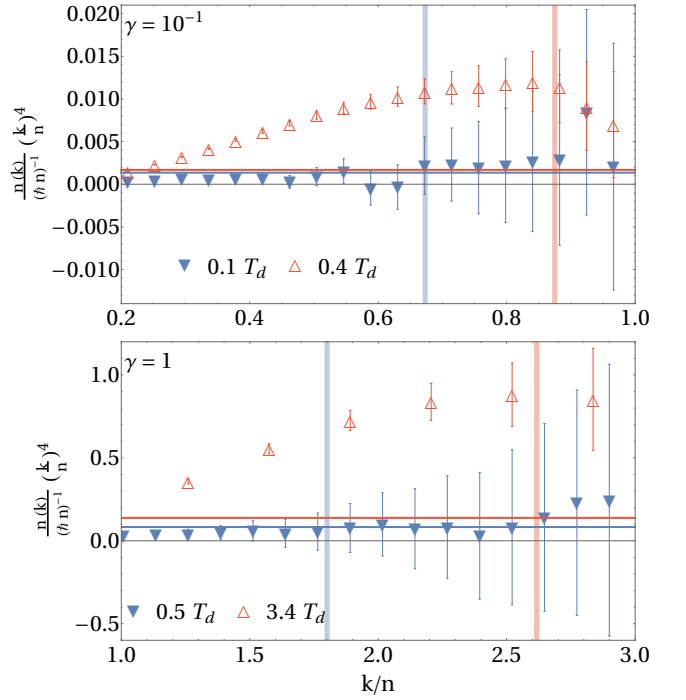


Figure 4. Scaled momentum distribution $n(k) k^4$ for $\gamma = 10^{-1}$ ($\gamma = 1$) in the upper (lower) panel. Solid (empty) symbols correspond to $T < T_A$ ($T > T_A$) and represent PIMC results. k_{\min} is denoted by vertical lines from low (left) to high (right) temperatures. Horizontal lines report $6n^3 b_3 / (\pi \hbar)$ of (9) obtained with TBA.

mal Bethe-Ansatz. Fig. 4 presents $n(k) k^4$, horizontal lines denote the coefficient of the Tan relation, from which the deviation of PIMC predictions is evident at $T > T_A$.

Consistently with our results for the short-distance OBDM, in Fig. 3, the complete tail for the distribution (9) and its minimal momentum k_{\min} are excellent approximations for any interaction strength and temperature [69], as shown by comparison with PIMC findings. While the Tan relation $\sim C/k^4$ in (9) is verified at low temperatures, it is thermally faded above the anomaly $T > T_A$. This fading crossover appears for any interaction strength [69] and at momenta close to k_{\min} , see Fig. 4, where the Tan relation is more important in (9). The deviation from the Tan law in Fig. 4 gets larger by raising the temperature [69]. However, the fading starts to occur at the anomaly temperature which is much lower than the one needed for the achievement of the Maxwell-Boltzmann classical gas regime, which is a limit described by Eq. (9).

Experimental Considerations.— 1D atomic Bose gases can be realized with a single optical tube trap [43] which allows for the exploration of temperatures below and above the hole anomaly. Spatial uniform density is achieved with a flat-box potential [75]. The interaction strength $\gamma \sim 1/(na)$ is tuned by changing the density n via the strongly confining radial potential [45, 48, 50] or by adjusting the scattering length a through Fano-Feshbach resonances [41, 76]. The temperature can be extracted from a single absorption image during

time-of-flight expansion with neural network [77]. The momentum distribution can also be measured [39–42, 47, 78–81].

Conclusions.— We built a unified theory which describes the entire contact-interaction and temperature crossover in a 1D repulsive Bose gas and provides a novel connection between excitations and correlations. We report that the hole anomaly, due to the thermal occupation of spectral states, induces an increase of the internal energy which is responsible for the high-temperature fading of the Tan relation in the large-momentum (short-distance) one-body correlations. Anomalies are ubiquitous in a variety of systems [22], even with interactions beyond the s -wave pairwise contact model, and behave as a second-order phase transition at the critical temperature. Our work suggests that the anomaly temperature may be identified in many systems [20, 63, 82–89] with the change from the quantum to thermal behavior in correlations even at short and not only at large [84, 90] distances.

G. D. R. received funding from the grant IJC2020-043542-I funded by MCIN/AEI/10.13039/501100011033 and by "European Union NextGenerationEU/PRTR". G.D.R., G.E.A. and J.B. were partially supported by the grant PID2020-113565GB-C21 funded by MCIN/AEI/10.13039/501100011033 and the grant 2021 SGR 01411 from the Generalitat de Catalunya. M.O. was supported by the NSF grant No. PHY-1912542.

* giulia.de.rosi@upc.edu

† grigori.astrakharchik@upc.edu

‡ jordi.boronat@upc.edu

- [1] S. Tan, *Energetics of a strongly correlated Fermi gas*, *Annals of Physics* **323**, 2952 (2008).
- [2] S. Tan, *Generalized virial theorem and pressure relation for a strongly correlated Fermi gas*, *Annals of Physics* **323**, 2987 (2008).
- [3] S. Tan, *Large momentum part of a strongly correlated Fermi gas*, *Annals of Physics* **323**, 2971 (2008).
- [4] A. Bulgac, *Entanglement entropy, single-particle occupation probabilities, and short-range correlations*, *Phys. Rev. C* **107**, L061602 (2023).
- [5] M. Olshanii and V. Dunjko, *Short-Distance Correlation Properties of the Lieb-Liniger System and Momentum Distributions of Trapped One-Dimensional Atomic Gases*, *Phys. Rev. Lett.* **91**, 090401 (2003).
- [6] M. Barth and W. Zwerger, *Tan relations in one dimension*, *Annals of Physics* **326**, 2544 (2011).
- [7] N. Matveeva and G. E. Astrakharchik, *One-dimensional multi-component Fermi gas in a trap: quantum Monte Carlo study*, *New Journal of Physics* **18**, 065009 (2016).
- [8] O. I. Păţu and A. Klümper, *Universal Tan relations for quantum gases in one dimension*, *Phys. Rev. A* **96**, 063612 (2017).
- [9] A. Minguzzi, P. Vignolo, and M. P. Tosi, *High-momentum tail in the Tonks gas under harmonic confinement*, *Physics Letters A* **294**, 222 (2002).
- [10] M. Rigol, *Finite-temperature properties of hard-core bosons confined on one-dimensional optical lattices*, *Phys. Rev. A* **72**, 063607 (2005).
- [11] F. Werner and Y. Castin, *General relations for quantum gases in two and three dimensions: Two-component fermions*, *Phys. Rev. A* **86**, 013626 (2012).
- [12] F. Werner and Y. Castin, *General relations for quantum gases in two and three dimensions. II. Bosons and mixtures*, *Phys. Rev. A* **86**, 053633 (2012).
- [13] E. Braaten, *Universal Relations for Fermions with Large Scattering Length*, in *The BCS-BEC Crossover and the Unitary Fermi Gas*, edited by W. Zwerger (Springer Berlin Heidelberg, Berlin, Heidelberg, 2012) pp. 193–231.
- [14] L. Pitaevskii and S. Stringari, *Bose-Einstein Condensation and Superfluidity*, International Series of Monographs on Physics (Oxford University Press, Oxford, 2016).
- [15] F. Qin and P. Zhang, *Universal relations for hybridized s - and p -wave interactions from spin-orbital coupling*, *Phys. Rev. A* **102**, 043321 (2020).
- [16] I. Bouchoule and J. Dubail, *Breakdown of Tan's Relation in Lossy One-Dimensional Bose Gases*, *Phys. Rev. Lett.* **126**, 160603 (2021).
- [17] H. Cayla, P. Massignan, T. Giamarchi, A. Aspect, C. I. Westbrook, and D. Clément, *Observation of $1/k^4$ -Tails after Expansion of Bose-Einstein Condensates with Impurities*, *Phys. Rev. Lett.* **130**, 153401 (2023).
- [18] G. Aupetit-Diallo, S. Musolino, M. Albert, and P. Vignolo, *High-momentum oscillating tails of strongly interacting one-dimensional gases in a box*, *Phys. Rev. A* **107**, L061301 (2023).
- [19] H. Hu, X.-J. Liu, and P. D. Drummond, *Universal contact of strongly interacting fermions at finite temperatures*, *New Journal of Physics* **13**, 035007 (2011).
- [20] J. T. Stewart, J. P. Gaebler, T. E. Drake, and D. S. Jin, *Verification of Universal Relations in a Strongly Interacting Fermi Gas*, *Phys. Rev. Lett.* **104**, 235301 (2010).
- [21] P. Makotyn, C. E. Klauss, D. L. Goldberger, E. A. Cornell, and D. S. Jin, *Universal dynamics of a degenerate unitary Bose gas*, *Nature Physics* **10**, 116 (2014).
- [22] G. De Rosi, R. Rota, G. E. Astrakharchik, and J. Boronat, *Hole-induced anomaly in the thermodynamic behavior of a one-dimensional Bose gas*, *SciPost Phys.* **13**, 035 (2022).
- [23] L. D. Landau and E. M. Lifshitz, *Statistical Physics: Vol. 5* (Elsevier Science, 2013).
- [24] N. P. Raju, E. Gmelin, and R. K. Kremer, *Magnetic-susceptibility and specific-heat studies of spin-glass-like ordering in the pyrochlore compounds $R_2\text{Mo}_2\text{O}_7$ ($R=\text{Y, Sm, or Gd}$)*, *Phys. Rev. B* **46**, 5405 (1992).
- [25] M. J. Harris, S. T. Bramwell, P. C. W. Holdsworth, and J. D. M. Champion, *Liquid-Gas Critical Behavior in a Frustrated Pyrochlore Ferromagnet*, *Phys. Rev. Lett.* **81**, 4496 (1998).
- [26] A. Tari, *The Specific Heat Of Matter At Low Temperatures* (World Scientific Publishing Company, 2003).
- [27] C. He, H. Zheng, J. F. Mitchell, M. L. Foo, R. J. Cava, and C. Leighton, *Low temperature Schottky anomalies in the specific heat of LaCoO_3 : Defect-stabilized finite spin states*, *Applied Physics Letters* **94**, 102514 (2009).
- [28] S. Lucas, K. Grube, C.-L. Huang, A. Sakai, S. Wunderlich, E. L. Green, J. Wosnitza, V. Fritsch, P. Gegenwart, O. Stockert, and H. v. Löhneysen, *Entropy Evolution in the Magnetic Phases of Partially Frustrated CePdAl* , *Phys. Rev. Lett.* **118**, 107204 (2017).
- [29] J. Brambleby, P. A. Goddard, J. Singleton, M. Jaime, T. Lancaster, L. Huang, J. Wosnitza, C. V. Topping, K. E. Carreiro, H. E. Tran, Z. E. Manson, and J. L. Manson, *Adiabatic physics of an exchange-coupled spin-dimer system: Magnetocaloric effect, zero-point fluctuations, and possible two-dimensional universal behavior*, *Phys. Rev. B* **95**, 024404 (2017).

- [30] E. Jurčišinová and M. Jurčišin, *Multipeak low-temperature behavior of specific heat capacity in frustrated magnetic systems: An exact theoretical analysis*, *Phys. Rev. E* **97**, 052129 (2018).
- [31] Z. Z. Yan, Y. Ni, C. Robens, and M. W. Zwierlein, *Bose polarons near quantum criticality*, *Science* **368**, 190 (2020).
- [32] M. J. H. Ku, A. T. Sommer, L. W. Cheuk, and M. W. Zwierlein, *Revealing the Superfluid Lambda Transition in the Universal Thermodynamics of a Unitary Fermi Gas*, *Science* **335**, 563 (2012).
- [33] D. C. Dender, P. R. Hammar, D. H. Reich, C. Broholm, and G. Aeppli, *Direct Observation of Field-Induced Incommensurate Fluctuations in a One-Dimensional $S = 1/2$ Antiferromagnet*, *Phys. Rev. Lett.* **79**, 1750 (1997).
- [34] P. R. Hammar, M. B. Stone, D. H. Reich, C. Broholm, P. J. Gibson, M. M. Turnbull, C. P. Landee, and M. Oshikawa, *Characterization of a quasi-one-dimensional spin-1/2 magnet which is gapless and paramagnetic for $g\mu_B H \lesssim J$ and $k_B T \ll J$* , *Phys. Rev. B* **59**, 1008 (1999).
- [35] T. Nakanishi and S. Yamamoto, *Intrinsic double-peak structure of the specific heat in low-dimensional quantum ferrimagnets*, *Phys. Rev. B* **65**, 214418 (2002).
- [36] C. Rüegg, K. Kiefer, B. Thielemann, D. F. McMorrow, V. Zapf, B. Normand, M. B. Zvonarev, P. Bouillot, C. Kollath, T. Giamarchi, S. Capponi, D. Poilblanc, D. Biner, and K. W. Krämer, *Thermodynamics of the Spin Luttinger Liquid in a Model Ladder Material*, *Phys. Rev. Lett.* **101**, 247202 (2008).
- [37] P. Bouillot, C. Kollath, A. M. Läuchli, M. Zvonarev, B. Thielemann, C. Rüegg, E. Orignac, R. Citro, M. Klanjšek, C. Berthier, M. Horvatić, and T. Giamarchi, *Statics and dynamics of weakly coupled antiferromagnetic spin- $\frac{1}{2}$ ladders in a magnetic field*, *Phys. Rev. B* **83**, 054407 (2011).
- [38] W. Xu and M. Rigol, *Universal scaling of density and momentum distributions in Lieb-Liniger gases*, *Phys. Rev. A* **92**, 063623 (2015).
- [39] S. Richard, F. Gerbier, J. H. Thywissen, M. Hugbart, P. Bouyer, and A. Aspect, *Momentum Spectroscopy of 1D Phase Fluctuations in Bose-Einstein Condensates*, *Phys. Rev. Lett.* **91**, 010405 (2003).
- [40] A. H. van Amerongen, J. J. P. van Es, P. Wicke, K. V. Kheruntsyan, and N. J. van Druten, *Yang-Yang Thermodynamics on an Atom Chip*, *Phys. Rev. Lett.* **100**, 090402 (2008).
- [41] F. Meinert, M. Panfil, M. J. Mark, K. Lauber, J.-S. Caux, and H.-C. Nägerl, *Probing the Excitations of a Lieb-Liniger Gas from Weak to Strong Coupling*, *Phys. Rev. Lett.* **115**, 085301 (2015).
- [42] B. Yang, Y.-Y. Chen, Y.-G. Zheng, H. Sun, H.-N. Dai, X.-W. Guan, Z.-S. Yuan, and J.-W. Pan, *Quantum criticality and the Tomonaga-Luttinger liquid in one-dimensional Bose gases*, *Phys. Rev. Lett.* **119**, 165701 (2017).
- [43] F. Salces-Carcoba, C. J. Billington, A. Putra, Y. Yue, S. Sugawa, and I. B. Spielman, *Equations of state from individual one-dimensional Bose gases*, *New J. Phys.* **20**, 113032 (2018).
- [44] S. Mistakidis, A. Volosniev, R. Barfknecht, T. Fogarty, T. Busch, A. Foerster, P. Schmelcher, and N. Zinner, *Few-body Bose gases in low dimensions—A laboratory for quantum dynamics*, *Physics Reports* **1042**, 1 (2023).
- [45] M. Olshanii, *Atomic Scattering in the Presence of an External Confinement and a Gas of Impenetrable Bosons*, *Phys. Rev. Lett.* **81**, 938 (1998).
- [46] M. Girardeau, *Relationship between Systems of Impenetrable Bosons and Fermions in One Dimension*, *Journal of Mathematical Physics* **1**, 516 (1960).
- [47] B. Paredes, A. Widera, V. Murg, O. Mandel, S. Fölling, I. Cirac, G. V. Shlyapnikov, T. W. Hänsch, and I. Bloch, *Tonks–Girardeau gas of ultracold atoms in an optical lattice*, *Nature* **429**, 277 EP (2004).
- [48] T. Kinoshita, T. Wenger, and D. S. Weiss, *Observation of a One-Dimensional Tonks–Girardeau Gas*, *Science* **305**, 1125 (2004).
- [49] B. Laburthe Tolra, K. M. O’Hara, J. H. Huckans, W. D. Phillips, S. L. Rolston, and J. V. Porto, *Observation of Reduced Three-Body Recombination in a Correlated 1D Degenerate Bose Gas*, *Phys. Rev. Lett.* **92**, 190401 (2004).
- [50] T. Kinoshita, T. Wenger, and D. S. Weiss, *Local Pair Correlations in One-Dimensional Bose Gases*, *Phys. Rev. Lett.* **95**, 190406 (2005).
- [51] E. Haller, M. Rabie, M. J. Mark, J. G. Danzl, R. Hart, K. Lauber, G. Pupillo, and H.-C. Nägerl, *Three-Body Correlation Functions and Recombination Rates for Bosons in Three Dimensions and One Dimension*, *Phys. Rev. Lett.* **107**, 230404 (2011).
- [52] T. Jacqmin, J. Armijo, T. Berrada, K. V. Kheruntsyan, and I. Bouchoule, *Sub-Poissonian Fluctuations in a 1D Bose Gas: From the Quantum Quasicondensate to the Strongly Interacting Regime*, *Phys. Rev. Lett.* **106**, 230405 (2011).
- [53] V. Guarrera, D. Muth, R. Labouvie, A. Vogler, G. Barontini, M. Fleischhauer, and H. Ott, *Spatiotemporal fermionization of strongly interacting one-dimensional bosons*, *Phys. Rev. A* **86**, 021601(R) (2012).
- [54] E. H. Lieb and W. Liniger, *Exact Analysis of an Interacting Bose Gas. I. The General Solution and the Ground State*, *Phys. Rev.* **130**, 1605 (1963).
- [55] E. H. Lieb, *Exact Analysis of an Interacting Bose Gas. II. The Excitation Spectrum*, *Phys. Rev.* **130**, 1616 (1963).
- [56] G. De Rosi, G. E. Astrakharchik, and S. Stringari, *Thermodynamic behavior of a one-dimensional Bose gas at low temperature*, *Phys. Rev. A* **96**, 013613 (2017).
- [57] C. N. Yang and C. P. Yang, *Thermodynamics of a One-Dimensional System of Bosons with Repulsive Delta-Function Interaction*, *Journal of Mathematical Physics* **10**, 1115 (1969).
- [58] C. P. Yang, *One-Dimensional System of Bosons with Repulsive δ -Function Interactions at a Finite Temperature T* , *Phys. Rev. A* **2**, 154 (1970).
- [59] E. Braaten, D. Kang, and L. Platter, *Universal Relations for Identical Bosons from Three-Body Physics*, *Phys. Rev. Lett.* **106**, 153005 (2011).
- [60] H. Yao, D. Clément, A. Minguzzi, P. Vignolo, and L. Sanchez-Palencia, *Tan’s Contact for Trapped Lieb-Liniger Bosons at Finite Temperature*, *Phys. Rev. Lett.* **121**, 220402 (2018).
- [61] G. De Rosi, P. Massignan, M. Lewenstein, and G. E. Astrakharchik, *Beyond-Luttinger-liquid thermodynamics of a one-dimensional Bose gas with repulsive contact interactions*, *Phys. Rev. Research* **1**, 033083 (2019).
- [62] G. De Rosi, R. Rota, G. E. Astrakharchik, and J. Boronat, *Correlation properties of a one-dimensional repulsive Bose gas at finite temperature*, *New J. Phys.* **25**, 043002 (2023).
- [63] G. E. Astrakharchik, D. M. Gangardt, Y. E. Lozovik, and I. A. Sorokin, *Off-diagonal correlations of the Calogero–Sutherland model*, *Phys. Rev. E* **74**, 021105 (2006).
- [64] R. P. Feynman, *Forces in Molecules*, *Phys. Rev.* **56**, 340 (1939).
- [65] V. A. Yurovsky, M. Olshanii, and D. S. Weiss, *Collisions, correlations, and integrability in atom waveguides* (Academic Press, 2008) pp. 61–138.
- [66] V. Dunjko and M. Olshanii, *A Hermite–Padé perspective on the renormalization group, with an application to the correlation function of Lieb-Liniger gas*, *Journal of Physics A: Mathematical and Theoretical* **44**, 055206 (2011).
- [67] M. Olshanii, V. Dunjko, A. Minguzzi, and G. Lang, *Connection between nonlocal one-body and local three-body correlations*

- of the Lieb-Liniger model, *Phys. Rev. A* **96**, 033624 (2017).
- [68] M. A. Cazalilla, *Bosonizing one-dimensional cold atomic gases*, *Journal of Physics B: Atomic, Molecular and Optical Physics* **37**, S1 (2004).
- [69] See Supplemental Material at [...] for additional results of the one-body density matrix and the momentum distribution, including the Maxwell-Boltzmann regime of the classical ideal gas at high temperatures. The Supplemental Material includes Refs. [62, 68, 91].
- [70] G. E. Astrakharchik and S. Giorgini, *Correlation functions and momentum distribution of one-dimensional Bose systems*, *Phys. Rev. A* **68**, 031602(R) (2003).
- [71] G. E. Astrakharchik and S. Giorgini, *Correlation functions of a Lieb-Liniger Bose gas*, *Journal of Physics B: Atomic, Molecular and Optical Physics* **39**, S1 (2006).
- [72] P. D. Drummond, P. Deuar, and K. V. Kheruntsyan, *Canonical Bose Gas Simulations with Stochastic Gauges*, *Phys. Rev. Lett.* **92**, 040405 (2004).
- [73] C. Mora and Y. Castin, *Extension of Bogoliubov theory to quasicondensates*, *Phys. Rev. A* **67**, 053615 (2003).
- [74] S. Cheng, Y.-Y. Chen, X.-W. Guan, W.-L. Yang, and H.-Q. Lin, *One-body dynamical correlation function of Lieb-Liniger model at finite temperature*, [arXiv:2211.00282](https://arxiv.org/abs/2211.00282) (2022).
- [75] B. Rauer, S. Erne, T. Schweigler, F. Cataldini, M. Tajik, and J. Schmiedmayer, *Recurrences in an isolated quantum many-body system*, *Science* **360**, 307 (2018).
- [76] C. Chin, R. Grimm, P. Julienne, and E. Tiesinga, *Feshbach resonances in ultracold gases*, *Rev. Mod. Phys.* **82**, 1225 (2010).
- [77] F. Møller, T. Schweigler, M. Tajik, J. a. Sabino, F. Cataldini, S.-C. Ji, and J. Schmiedmayer, *Thermometry of one-dimensional Bose gases with neural networks*, *Phys. Rev. A* **104**, 043305 (2021).
- [78] N. Fabbri, D. Clément, L. Fallani, C. Fort, and M. Inguscio, *Momentum-resolved study of an array of one-dimensional strongly phase-fluctuating Bose gases*, *Phys. Rev. A* **83**, 031604(R) (2011).
- [79] J. M. Wilson, N. Malvania, Y. Le, Y. Zhang, M. Rigol, and D. S. Weiss, *Observation of dynamical fermionization*, *Science* **367**, 1461 (2020).
- [80] N. Malvania, Y. Zhang, Y. Le, J. Dubail, M. Rigol, and D. S. Weiss, *Generalized hydrodynamics in strongly interacting 1D Bose gases*, *Science* **373**, 1129 (2021).
- [81] Y. Le, Y. Zhang, S. Gopalakrishnan, M. Rigol, and D. S. Weiss, *Observation of hydrodynamization and local prethermalization in 1D Bose gases*, *Nature* **618**, 494 (2023).
- [82] G. E. Astrakharchik, J. Boronat, J. Casulleras, and S. Giorgini, *Beyond the Tonks-Girardeau Gas: Strongly Correlated Regime in Quasi-One-Dimensional Bose Gases*, *Phys. Rev. Lett.* **95**, 190407 (2005).
- [83] E. Haller, M. Gustavsson, M. J. Mark, J. G. Danzl, R. Hart, G. Pupillo, and H.-C. Nägerl, *Realization of an Excited, Strongly Correlated Quantum Gas Phase*, *Science* **325**, 1224 (2009).
- [84] J. Fischer, I. G. Savenko, M. D. Fraser, S. Holzinger, S. Brodbeck, M. Kamp, I. A. Shelykh, C. Schneider, and S. Höfling, *Spatial Coherence Properties of One Dimensional Exciton-Polariton Condensates*, *Phys. Rev. Lett.* **113**, 203902 (2014).
- [85] O. Benhar and G. De Rosi, *Superfluid Gap in Neutron Matter from a Microscopic Effective Interaction*, *J Low Temp Phys* **189**, 250 (2017).
- [86] G. De Rosi, G. E. Astrakharchik, and P. Massignan, *Thermal instability, evaporation, and thermodynamics of one-dimensional liquids in weakly interacting Bose-Bose mixtures*, *Phys. Rev. A* **103**, 043316 (2021).
- [87] J. Hofmann and W. Zwerger, *Universal relations for dipolar quantum gases*, *Phys. Rev. Res.* **3**, 013088 (2021).
- [88] K.-Y. Li, Y. Zhang, K. Yang, K.-Y. Lin, S. Gopalakrishnan, M. Rigol, and B. L. Lev, *Rapidity and momentum distributions of one-dimensional dipolar quantum gases*, *Phys. Rev. A* **107**, L061302 (2023).
- [89] A. Del Maestro, N. Nichols, T. Prisk, G. Warren, and P. E. Sokol, *Experimental realization of one dimensional helium*, *Nature Comm.* **13**, 3168 (2022).
- [90] P. A. Murthy, I. Boettcher, L. Bayha, M. Holzmann, D. Kedar, M. Neidig, M. G. Ries, A. N. Wenz, G. Zürn, and S. Jochim, *Observation of the Berezinskii-Kosterlitz-Thouless Phase Transition in an Ultracold Fermi Gas*, *Phys. Rev. Lett.* **115**, 010401 (2015).
- [91] J. Esteve, J.-B. Trebbia, T. Schumm, A. Aspect, C. I. Westbrook, and I. Bouchoule, *Observations of Density Fluctuations in an Elongated Bose Gas: Ideal Gas and Quasicondensate Regimes*, *Phys. Rev. Lett.* **96**, 130403 (2006).

Supplemental Material for “Thermal fading of the $1/k^4$ -tail of the momentum distribution induced by the hole anomaly”

Giulia De Rosi,^{1,*} Grigori E. Astrakharchik,^{1,2,†} Maxim Olshanii,³ and Jordi Boronat^{1,‡}

¹*Departament de Física, Universitat Politècnica de Catalunya, Campus Nord B4-B5, 08034 Barcelona, Spain*

²*Departament de Física Quàntica i Astrofísica, Facultat de Física, Universitat de Barcelona, E-08028 Barcelona, Spain*

³*Department of Physics, University of Massachusetts Boston, Boston Massachusetts 02125, USA*

(Dated: February 21, 2024)

In this Supplemental Material, we show with symbols the additional exact Path Integral Monte Carlo (PIMC) results for the one-body density matrix (OBDM) (Sec. S1) and the momentum distribution (Sec. S2) in a one-dimensional Bose gas with contact repulsive interaction. We consider different characteristic values of the interaction strength γ and temperature crossing the hole-anomaly threshold T_A (see Fig. 1 in the main text) rescaled in units of the quantum degeneracy value $T_d = \hbar^2 n^2 / (2mk_B)$. Our findings also include the Maxwell-Boltzmann (MB) regime describing the classical ideal gas at very high temperatures.

S1. ONE-BODY DENSITY MATRIX

In Figs. S1-S3, we report the one-body density matrix $g_1(x)$. We compare the complete short-distance expansion of the OBDM (Eq. (4) of the main text), which is denoted by colored solid lines, with the same result but without the non-analytic cubic term (whose coefficient is b_3) and corresponding to black dashed lines. Both curves are calculated with exact thermal Bethe-Ansatz (TBA) method. The maximal distance $x_{\max} = (\xi^{-1} + \sigma^{-1})^{-1}$ (Eq. (7) in the main text) for the validity of the expansion at short range is represented with vertical lines. In the lowest panel of each figure, PIMC results have been previously checked to agree with the analytical Maxwell-Boltzmann classical gas limit $g_1(x)_{\text{MB}} = ne^{-x^2/(2\sigma^2)}$ [1].

In Fig. S1, we present the case of weak interactions with $\gamma = 10^{-1}$. Each panel corresponds to different physical thermal regimes in order of increasing temperature values: hole-anomaly (upper panel), intermediate (middle) and MB (lower) regime.

Fig. S2 reports the intermediate value of the interaction strength $\gamma = 1$ in the anomaly (upper panel) and MB (lower) regime.

Fig. S3 shows $\gamma = 10$ for strong interactions, in the anomaly (upper panel), virial hard-core (middle) and MB (lower) regime.

Our approximation for x_{\max} (Eq. (7) in the main text) is valid along the whole interaction and temperature crossover of the system, as witnessed by comparison between the complete short-range expansion of the OBDM (Eq. (4) of the main text) and the corresponding PIMC results.

The non-analytic cubic term, which is more important in the short-range behavior of the OBDM at distances approaching x_{\max} , is thermally faded at temperatures above the hole-anomaly threshold $T > T_A$ in any interacting regime, as reported by the comparison between the colored solid and black dashed lines. This fading mechanism is a smooth crossover and not an abrupt change occurring exactly at the hole-anomaly temperature T_A .

S2. MOMENTUM DISTRIBUTION

In Figs. S4-S6, we present the complete k -dependence for the momentum distribution $n(k)$, by exploring all possible regimes in the interaction-temperature crossover. For any value of the interaction strength γ , dashed lines in the lowest panels denote the analytical limit $n(k)_{\text{MB}} = \sigma / (\hbar\sqrt{2\pi}) e^{-\sigma^2 k^2/2}$, describing the classical gas at high temperatures, and which exhibits an excellent agreement with PIMC findings.

In Fig. S4, we present the case of weak interactions, $\gamma = 10^{-1}$, around the hole-anomaly (upper panel), intermediate temperatures (middle) and Maxwell-Boltzmann classical (lower) regime.

In Fig. S5, we report the intermediate value for the interaction strength $\gamma = 1$. Each panel corresponds to different thermal regimes: very low temperatures and small momenta (upper panel), anomaly (middle) and MB (lower) regime.

Fig. S6 shows $\gamma = 10$ for strong repulsions, in the anomaly (upper panel), virial hard-core (middle) and MB (lower) regime.

At zero temperature and weak interparticle repulsion $\gamma \ll 1$, the occupation of the zero-momentum state features a power-law divergence with the particle number N : $n(k=0) \propto N^{1-1/(2K)}$ where $K \geq 1$ is the Luttinger parameter [2]. This is a remnant of the Bose-Einstein condensation, which is reached only asymptotically for $\gamma \rightarrow 0$ ($K \rightarrow \infty$), where $n(k=0) \propto N$. At finite temperature, the peak in $n(k=0)$ is smeared and the divergence is removed. The peak gets smaller and broader with the increase of temperature and interaction strength, see Figs. S4-S6. For $\gamma = 10^{-1}$ and low temperatures, the peak is high, consistently with

the presence of a quasicondensate [3], but it does not show a delta-function behavior typical of a true condensate in higher spatial dimensions. The thermal disappearance of the quasicondensate has been found even in other correlation properties [1].

In Fig. S7, we report the distribution at large momenta k , for a weakly-repulsive gas $\gamma = 10^{-1}$ and temperatures below the anomaly threshold $T < T_A$ (upper panel) and at $T > T_A$ in the intermediate thermal regime (lower). We compare the complete tail of the momentum distribution (Eq. (9) of the main text), which is denoted by colored solid lines, with the same result with $b_3 = 0$ and corresponding to the black dashed lines. Both curves are calculated with exact thermal Bethe-Ansatz method. The minimum momentum $k_{\min} = x_{\max}^{-1} = (\xi^{-1} + \sigma^{-1})$ for the validity of the complete tail corresponds to vertical lines. Similar results in other interacting regimes are presented in the main text.

Consistently with the behavior of the short-distance OBDM in Sec. S1, k_{\min} is valid for any interaction strength and temperature, as shown by the comparison between the complete tail (Eq. (9) of the main text) and exact PIMC results in Fig. S7 and similar plots in the main text. We also notice that the new analytical approximation for the large-momentum tail of the distribution (Eq. (9) of the main text) is valid in any interacting and thermal regime as it agrees with the corresponding PIMC data at momenta larger than the minimal value $|k| \gtrsim k_{\min}$.

In Fig. S8, we present the scaled momentum distribution $n(k)k^4$ to make even more visible the thermal fading of the Tan relation \mathcal{C}/k^4 (where \mathcal{C} is the Tan contact) in the large- k tail at high temperatures. In the upper panel, we consider the strongly-interacting regime $\gamma = 10$ and results for $T < T_A$ ($T > T_A$) reported with solid (empty) symbols. In the lower panel, we show instead the weakly-repulsive system with $\gamma = 10^{-1}$ and in the intermediate thermal regime $T > T_A$. k_{\min} is denoted by vertical lines. Horizontal lines correspond to the coefficient of the Tan-relation tail $6n^3b_3/(\pi\hbar) \sim \mathcal{C}$ (see Eq. (9) of the main text) which is computed with thermal Bethe-Ansatz method. Additional findings for other values of the interaction strength γ and temperatures are reported in the main text.

The thermal fading of the Tan relation in the tail of the momentum distribution takes place for any finite contact-interaction strength and temperatures above the hole-anomaly threshold $T > T_A$ including the typical values of the classical gas regime. The fading crossover is more evident by raising the temperature and at momenta close to k_{\min} , where the contribution of the Tan relation is important in the analytical approximation for the complete tail (Eq. (9) of the main text).

* giulia.de.rosi@upc.edu

† grigori.astrakharchik@upc.edu

‡ jordi.boronat@upc.edu

- [1] G. De Rosi, R. Rota, G. E. Astrakharchik, and J. Boronat, *Correlation properties of a one-dimensional repulsive Bose gas at finite temperature*, *New J. Phys.* **25**, 043002 (2023).
- [2] M. A. Cazalilla, *Bosonizing one-dimensional cold atomic gases*, *Journal of Physics B: Atomic, Molecular and Optical Physics* **37**, S1 (2004).
- [3] J. Esteve, J.-B. Trebbia, T. Schumm, A. Aspect, C. I. Westbrook, and I. Bouchoule, *Observations of Density Fluctuations in an Elongated Bose Gas: Ideal Gas and Quasicondensate Regimes*, *Phys. Rev. Lett.* **96**, 130403 (2006).

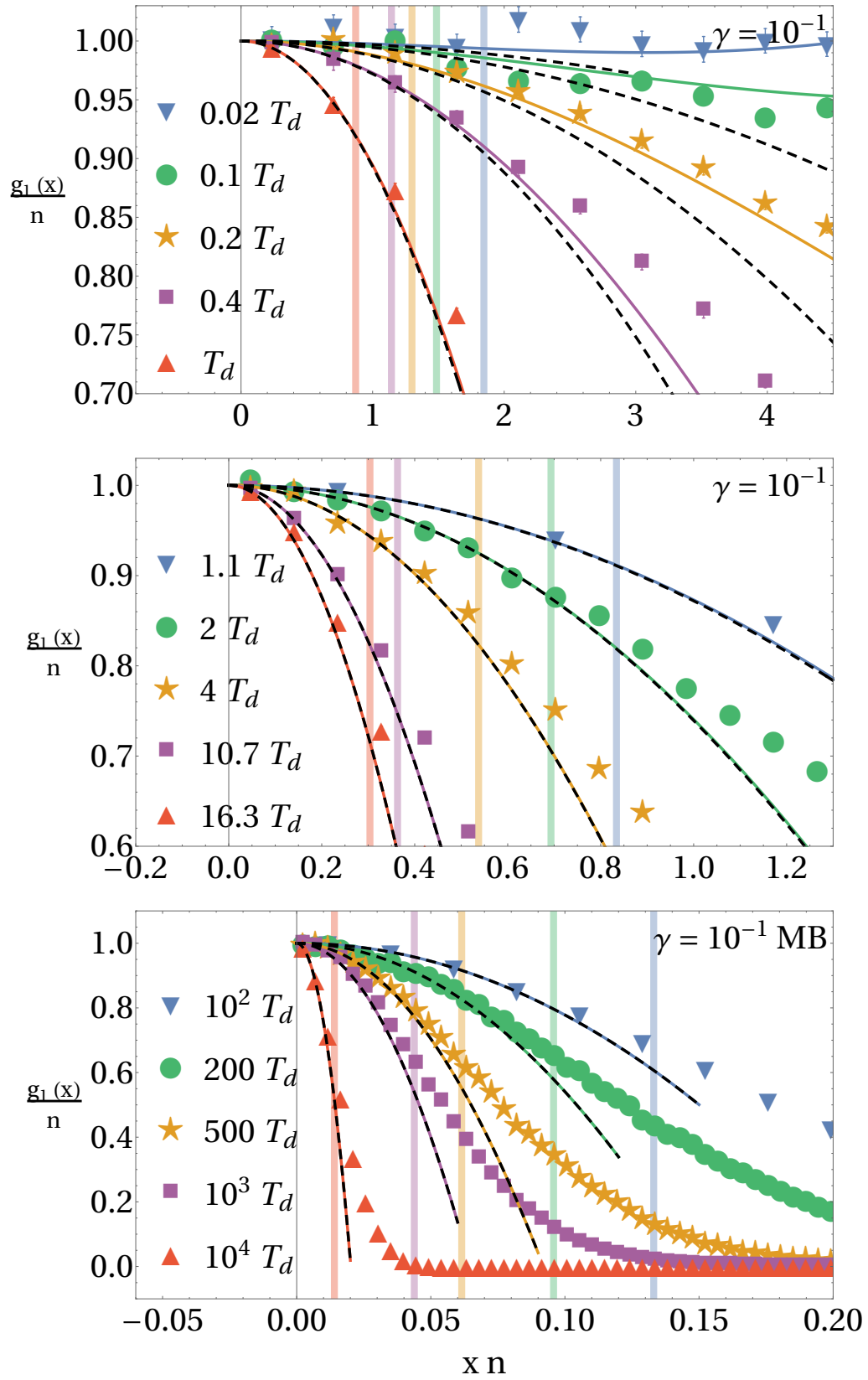


Figure S1. One-body density matrix $g_1(x)/n$ as a function of the interparticle distance xn (n is the density) for weak interactions $\gamma = 10^{-1}$. Different values of temperature in units of the quantum degeneracy value $T_d = \hbar^2 n^2 / (2mk_B)$ are reported. Symbols denote exact Path Integral Monte Carlo results and their sizes are larger than the statistical error bars in some cases. Solid lines represent the complete expansion at short distances (Eq. (4) of the main text) calculated with exact thermal Bethe-Ansatz method. Dashed black lines correspond to the same, but without the non-analytic cubic term (i.e. with $b_3 = 0$). All curves are reported in increasing order of the temperature from small (top) to large (bottom) values in each panel. The maximum distance for the validity of the short-range expansion $x_{\max} n = (\xi^{-1} + \sigma^{-1})^{-1} n$ is represented by vertical lines from low (right) to high (left) temperature in each panel. The lowest panel corresponds to the Maxwell-Boltzmann regime of the classical ideal gas at very high temperatures.

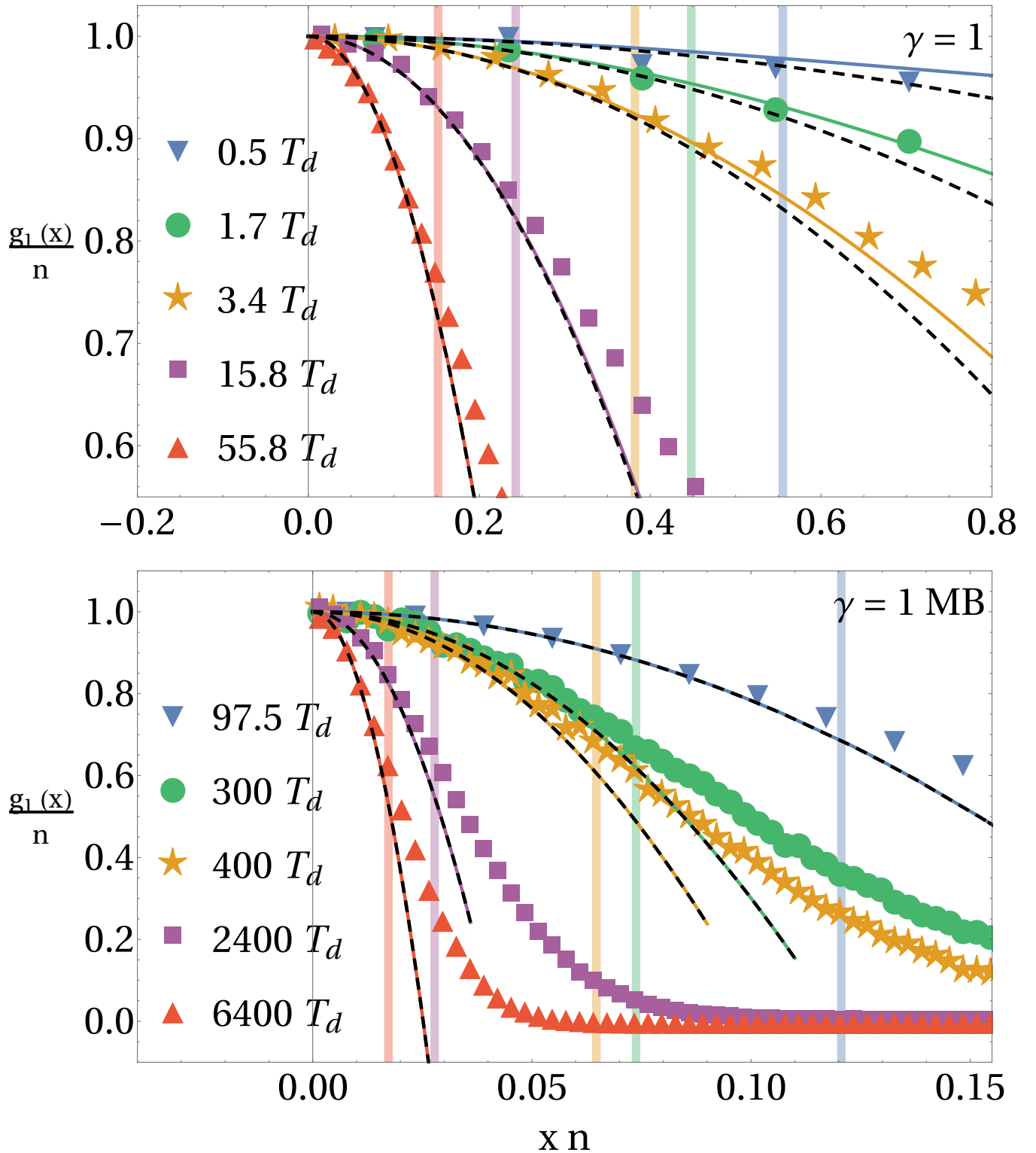


Figure S2. OBDM for the intermediate interaction strength $\gamma = 1$, similarly as in Fig. S1. Symbols denote PIMC results. Solid lines represent the complete short-distance expansion (Eq. (4) of the main text) calculated with TBA. Dashed black lines correspond to the same expansion, but without the non-analytic cubic term (i.e. with $b_3 = 0$). All curves are reported for increasing temperature from small (top) to large (bottom) values in each panel. The maximum distance $x_{\max} n$ is represented by vertical lines from low (right) to high (left) temperature in each panel. The lower panel refers to the MB regime of the classical gas limit at very high temperatures.

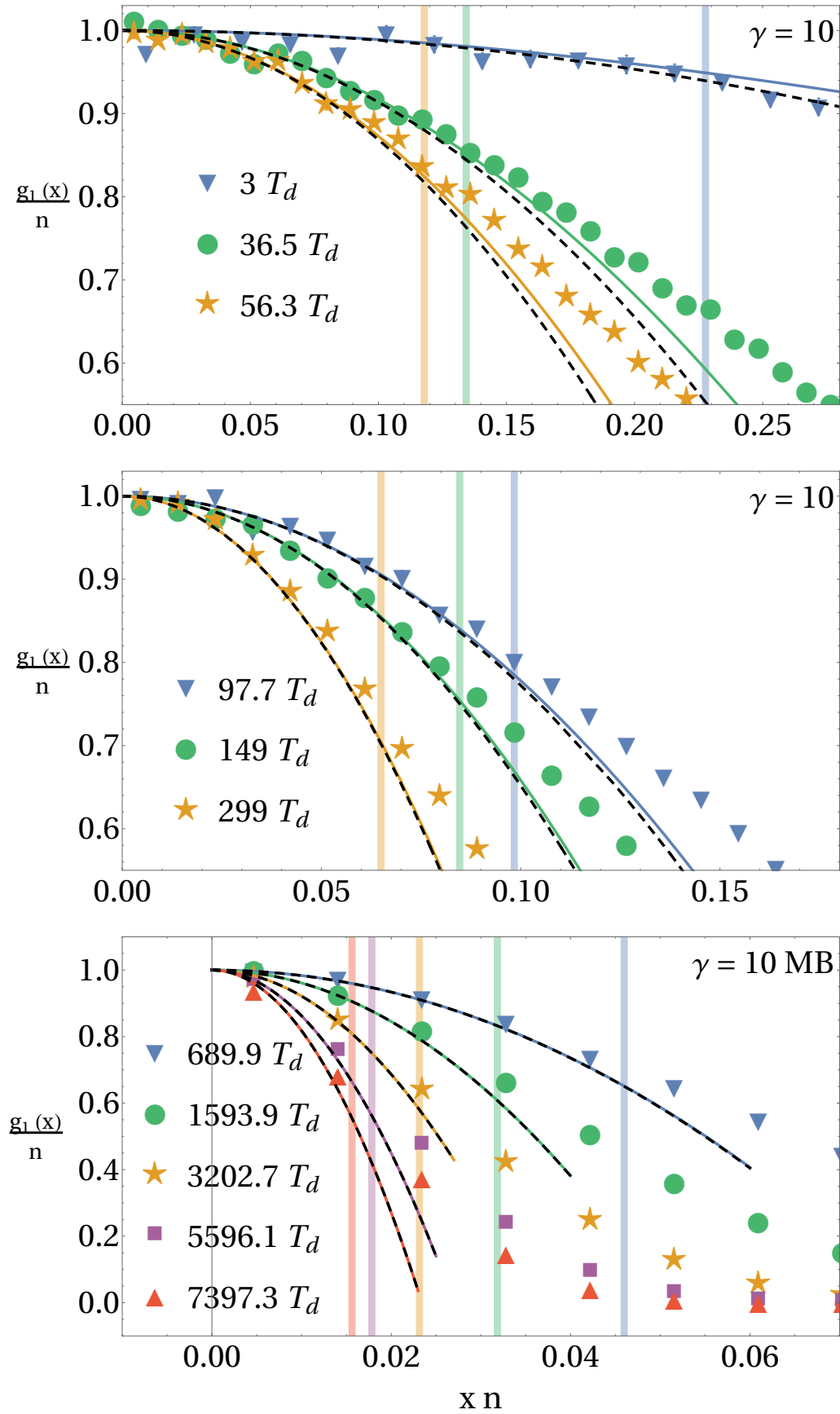


Figure S3. OBDM for strong interactions $\gamma = 10$, similarly as in Fig. S1. Symbols correspond to PIMC results. Solid lines represent the complete expansion at short distances (Eq. (4) of the main text) calculated with TBA. Dashed black lines correspond to the same, but without the non-analytic cubic term (i.e. with $b_3 = 0$). All curves are reported in increasing order of the temperature from small (top) to large (bottom) values in each panel. The maximum distance $x_{\max} n$ is represented by vertical lines from low (right) to high (left) temperature in each panel. The lowest panel refers to the MB classical gas regime at very high temperatures.

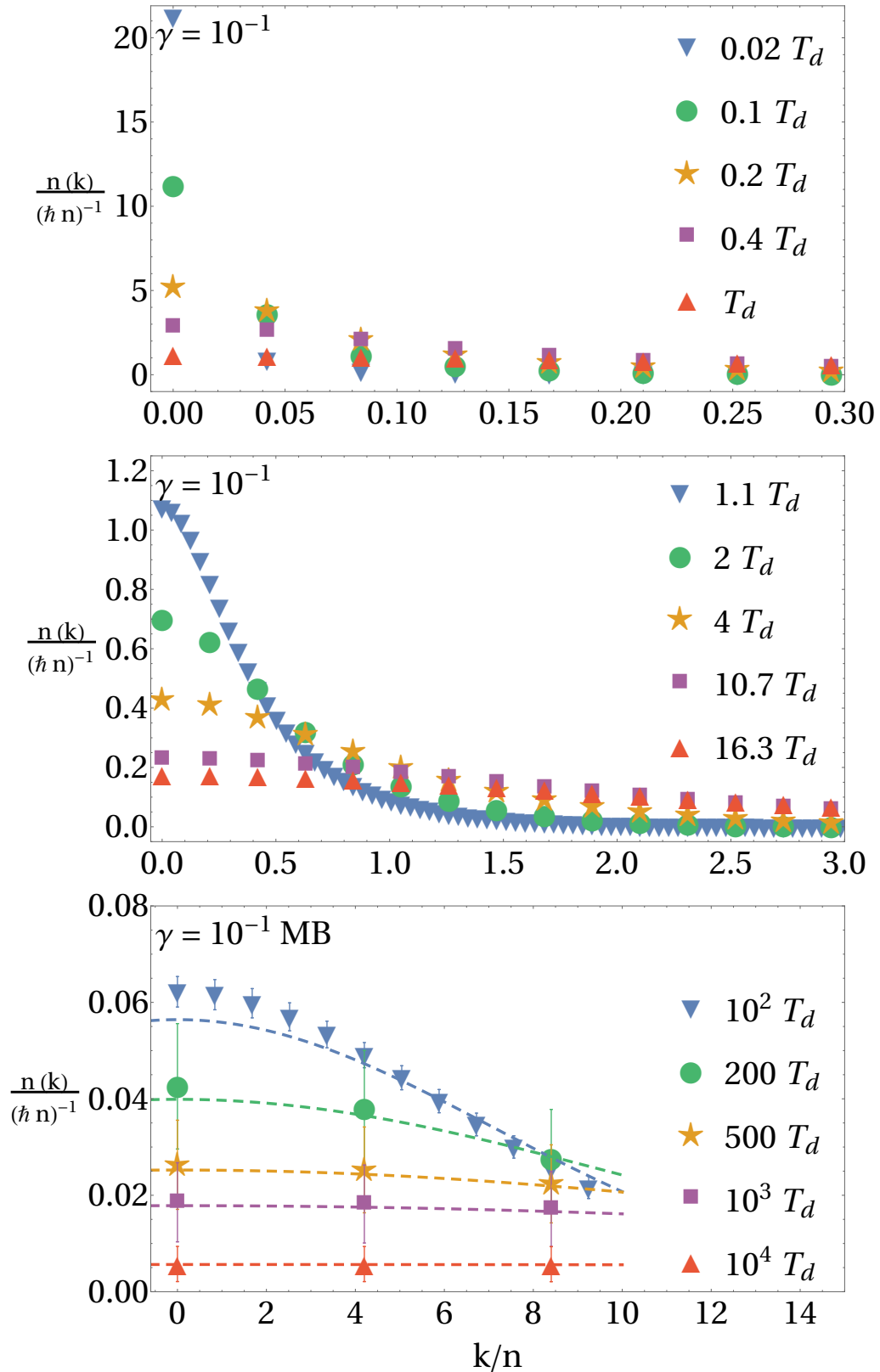


Figure S4. Momentum distribution $n(k)/(\hbar n)^{-1}$ as a function of the momentum k/n (n is the density). The weakly-interacting regime with $\gamma = 10^{-1}$ is considered. Temperature is reported in units of the quantum degeneracy value $T_d = \hbar^2 n^2 / (2mk_B)$. Symbols denote exact Path Integral Monte Carlo results and their sizes are larger than the statistical error bars in some cases. Dashed lines represent the Maxwell-Boltzmann limit $n(k)_{\text{MB}}/(\hbar n)^{-1} = \sigma/(\hbar\sqrt{2\pi}) e^{-\sigma^2 k^2/2}/(\hbar n)^{-1}$ of the classical gas at high temperatures and are reported in increasing order of the temperature from small (top) to large (bottom) values in the legend.

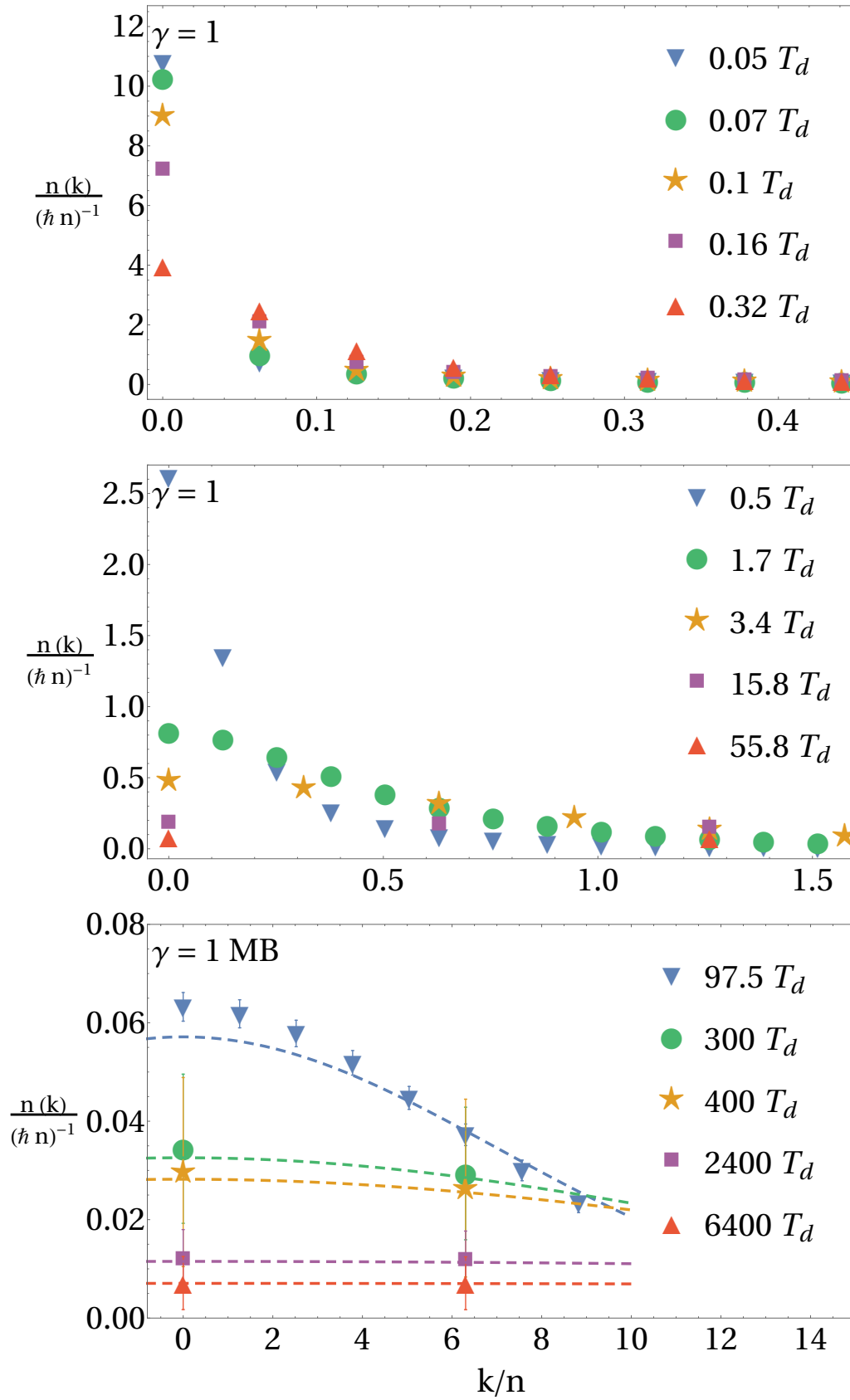


Figure S5. Momentum distribution for the intermediate interaction strength $\gamma = 1$, similarly as in Fig. S4. Symbols represent PIMC results. Dashed lines denote the limit $n(k)_{\text{MB}}/(\hbar n)^{-1}$ of the classical gas at very high temperatures and are reported in order of increasing temperature from small (top) to large (bottom) values in the lowest panel.

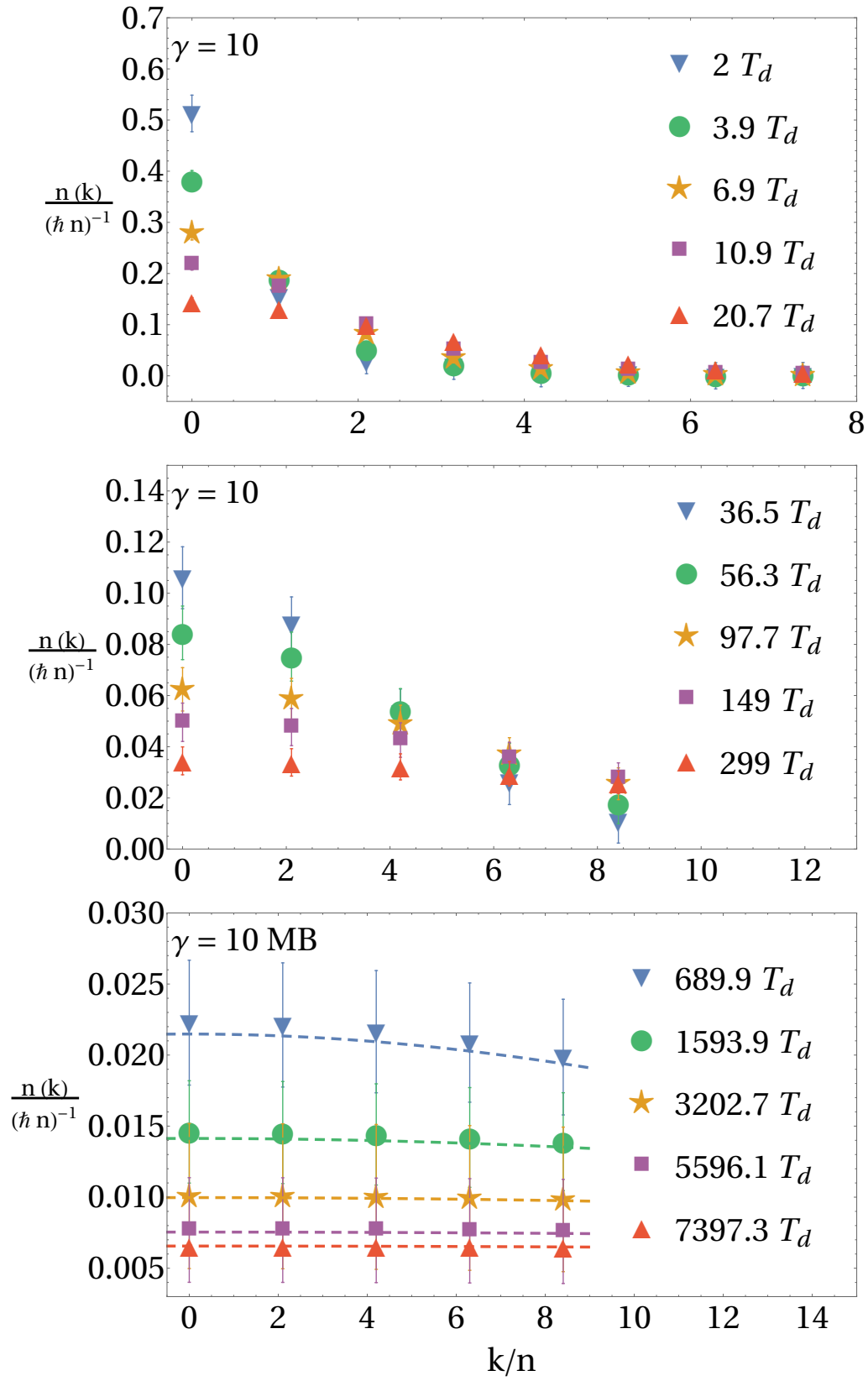


Figure S6. Momentum distribution for strong interactions, $\gamma = 10$, similarly as in Fig. S4. Symbols correspond to PIMC results. Dashed lines represent the limit $n(k)_{\text{MB}} / (\hbar n)^{-1}$ of the classical gas at high temperatures and are reported from low (top) to high (bottom) temperatures in the lowest panel.

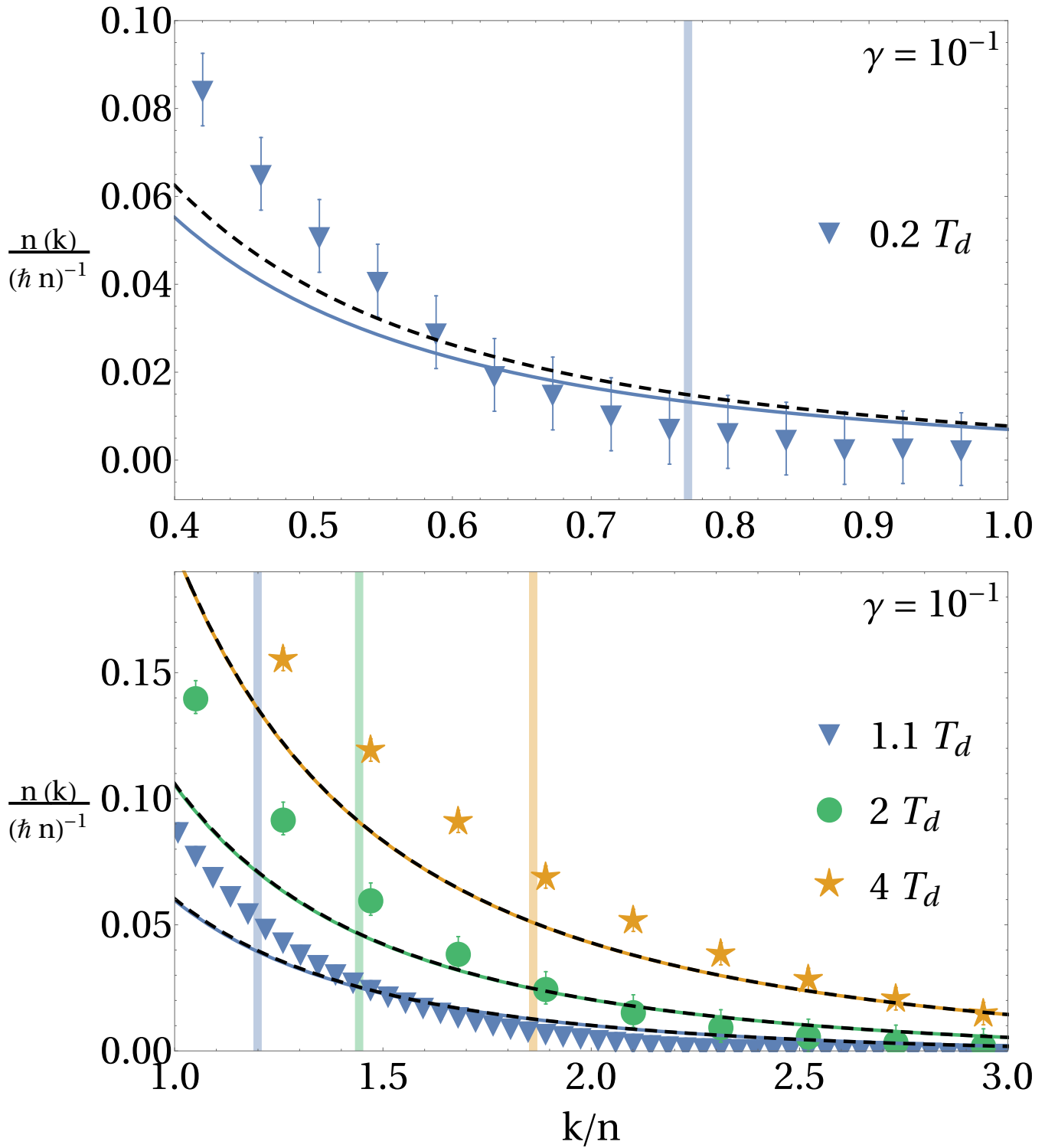


Figure S7. Large-momentum behavior of the momentum distribution $n(k)$ in the weakly-interacting regime $\gamma = 10^{-1}$ and for temperatures below the hole-anomaly threshold $T < T_A$ (upper panel) and $T > T_A$ (lower) in units of the quantum degeneracy value $T_d = \hbar^2 n^2 / (2mk_B)$. Symbols correspond to exact Path Integral Monte Carlo results. Colored solid lines represent the complete tail at large momenta (Eq. (9) of the main text) calculated with exact thermal Bethe-Ansatz method. Dashed black lines correspond to the same, but with $b_3 = 0$. All curves are reported in increasing order of the temperature from small (bottom) to large (top) values in the lower panel. The minimum momentum for the validity of the distribution tail $k_{\min} = x_{\max}^{-1} = (\xi^{-1} + \sigma^{-1})$ is represented with vertical lines with increasing order of temperature from small (left) to large (right) values.

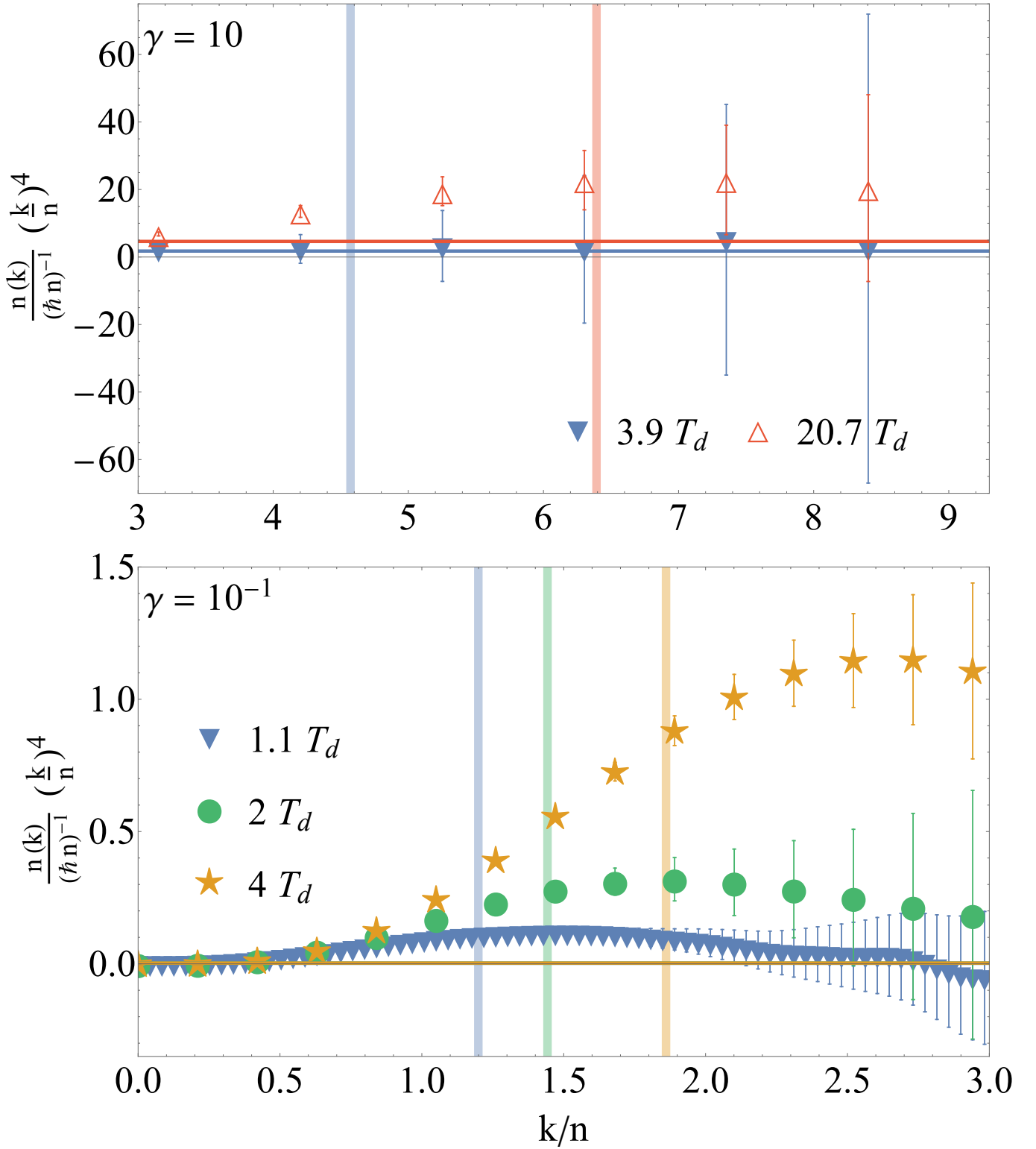


Figure S8. Scaled momentum distribution $n(k) k^4$ as a function of the momentum k . In the upper panel, we report $\gamma = 10$ for the strongly-interacting gas at temperatures below $T < T_A$ (solid symbols) and above $T > T_A$ (empty) the hole-anomaly threshold T_A . In the lower panel, we show results for weak interactions $\gamma = 10^{-1}$ in the intermediate thermal regime with $T > T_A$. Symbols correspond to exact Path Integral Monte Carlo results. The minimum momentum for the distribution tail k_{\min} is represented with vertical lines with increasing order of temperature from small (left) to large (right) values in each panel. Horizontal lines report the coefficient of the Tan relation $6n^3 b_3 / (\pi \hbar)$ (see Eq. (9) of the main text) calculated with exact thermal Bethe-Ansatz technique and they overlap at different temperatures in the lower panel.